

Copying the Cochlea: Micromachined Biomimetic Acoustic Sensors

Robert D. White, Robert Littrell, and Karl Grosh

ABSTRACT

In this work, a micromachined acoustic sensor system inspired by the mammalian cochlea is demonstrated. This type of system is capable of acoustic sensing and simultaneous mechanical frequency analysis. The implementation described here uses a capacitive sensing scheme to produce 32 channels of filtered output. The main sensor structure is a 3 cm long, 1.2 μm thick, LPCVD Si_3N_4 /Polysilicon/ Si_3N_4 membrane which tapers exponentially in width from 140 μm to 1.82 mm. The membrane interacts with a fluid-filled duct. The current design responds with 0.2 nm of motion per Pascal of driving pressure in the 10-60 kHz band as measured by laser vibrometry. The 32 on-chip capacitive sensors which were incorporated into the device exhibited sensitivities of 0.05-0.35 mV/Pa (at the preamp output). A cochlear-like frequency-position map is demonstrated in the laser vibrometry measurements, but has not yet been shown in the on-chip measurements.

INTRODUCTION

The mammalian cochlea, the organ responsible for hearing, achieves remarkable acoustic transduction characteristics in a very compact design. The mechanics of the fluid-structure interaction within the cochlea create a sensitive real time frequency analyzer, delivering approximately 3000 channels of frequency information. The human cochlea operates over a 3 decade band in frequency, 120 dB of dynamic range, and can distinguish tones which differ less than 0.5%. These characteristics are superb, particularly when one considers that the cochlea operates on approximately 14 μW of power [1, 2] and takes up only 1 cm^3 of volume [3]. Can we build an engineered version?

Researchers in cochlear mechanics have produced a number of physical models of the cochlea, most of which are of an exaggerated size [4, 5]. In recent years, a number of life-sized, micromachined models have been reported [6-9]. These devices demonstrate the ability to achieve passive cochlear-like acoustic filtering in a life-size engineered cochlea. The device described in this abstract is fully micromachined and incorporates integrated sensing elements. Development of the current version of the cochlear-like sensor system has gone through a number of stages which are described in previous publications by the authors [10-13]. We refer to our device as a micro-Cochlear Analogue Transducer (μCAT).

The μ CAT could potentially be applied for structural health monitoring applications as a combined sensor/analysis system for acoustic emissions (AE) in structures [14, 15]. It would be most applicable for situations in which the spectral content of the acoustic signal must be analyzed in a low power process. There is also a potential natural synergy between the biomimetic sensory design of the μ CAT and the biomimetic neural net analysis methods currently under investigation in the structural health monitoring community [16, 17].

BIOMIMETIC DESIGN

The design of the μ CAT is derived from the physiology of the inner ear. For an extensive review of cochlear physiology, experimental results, and models, see Robles and Ruggero [18], Dallos, Popper and Fay (editors) [3], and C. Daniel Geisler [19]. The cochlea is a spiral shaped organ consisting mainly of three ducts filled with endolymph and perilymph, two ion-rich water-like fluids. The three ducts, the scala timpani, scala media, and scala vestibuli, are separated by Reissner's membrane and the basilar membrane (BM), respectively. Acoustic energy is injected into the scala vestibuli via the stapes bone. The stapes acts like a rigid input piston, and is driven by environmental sound via the middle and outer ear. A fluid-structure wave is excited by the motion of the stapes, and travels down the length of the cochlear spiral, interacting with the microstructures in the organ of Corti (OoC) and the BM. The effective mass and stiffness of the OoC/BM structure change along the length of the cochlear spiral. Due to this changing acoustic impedance, high frequency sounds excite amplified BM motion near the base of the cochlea, and low frequency sounds excite motion near the apex.

The simplest analogy to the mechanical structure of the cochlea is a single straight fluid-filled duct (representing the fluid-filled scala) bounded along one side by a tapered membrane (representing the variable structural impedance of the BM and OoC). This mechanical structure forms the basis of the μ CAT design. In addition, we incorporate capacitive sensing elements along the length of the membrane (representing the sensory inner hair cells). This is accomplished by using a conducting membrane (highly boron doped polysilicon) and bonding on a glass die with patterned Cr/Pt electrodes arrayed along its length. These electrodes form a series of parallel plate capacitors with the membrane. Each electrode is a separate channel of output, measuring vibration of the section of membrane under that electrode.

Figure 1 shows the dimensioned design. The length of the fluid filled duct, 3.5 cm, is similar to the length of an uncoiled human cochlea (4 cm). The fluid chamber height, 0.475 mm, lies within the range of human scala height (0.1-2 mm). The volume compliance of the variable width membrane, $10^{-11} - 10^{-14} \text{ m}^4/\text{N}$ is similar to the human BM, $10^{-10} - 10^{-14} \text{ m}^4/\text{N}$. One notable difference between the μ CAT and the cochlea is the viscosity of the filling fluid. In our design, 200 cSt silicone oil was used to add sufficient damping to prevent wave reflections. The endolymph and perilymph

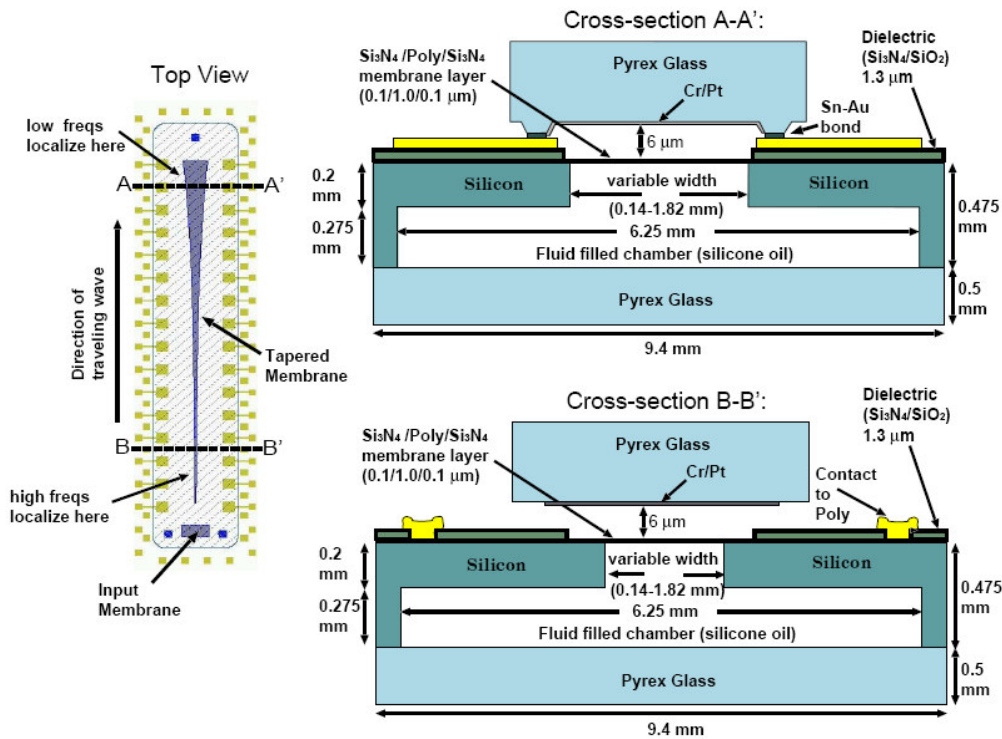


Figure 1: Schematic of the μ CAT design showing a top view (left) and two cross-sections (right).

in the cochlea have viscosities similar to water (1 cSt). In addition, the width of the fluid duct in the μ CAT, 6.25 mm , is greater than the physiological width ($1-2 \text{ mm}$). It should also be noted that in the cochlea the height and width of the fluid duct vary with longitudinal position down the spiral; in the μ CAT the duct height is constant due to fabrication limitations.

MICROFABRICATION

Microfabrication proceeds as follows. The starting substrates are 100 mm diameter, $475 \mu\text{m}$ thick, $\langle 100 \rangle$ oriented, p-type (boron) ($1-10 \text{ Ohm}\cdot\text{cm}$) silicon wafers. An SiO_2 film $2 \mu\text{m}$ thick is grown by pyrogenic oxidation. 100 nm of stoichiometric silicon nitride and $1.1 \mu\text{m}$ of low stress polysilicon are then deposited using low pressure chemical vapor deposition (LPCVD). The polysilicon film is doped using solid source boron diffusion at $1175 \text{ }^\circ\text{C}$. The borosilicate glass (BSG) that grows during doping is stripped in hydrofluoric acid (HF). Three dielectric films are then deposited by LPCVD: 100 nm of Si_3N_4 , 800 nm of SiO_2 , and finally 250 nm of Si_3N_4 . The membrane structure will eventually be built out of the central nitride/polysilicon/nitride structural laminate ($100 \text{ nm}/1 \mu\text{m}/100 \text{ nm}$) which has approximately 40 MPa net tensile stress (as measured by wafer curvature) and a sheet resistivity of $10-50 \text{ } \Omega/\text{square}$. Control of the film stress is critical for device design. A compressive membrane will buckle, a highly tensile membrane will exhibit much lower volume compliance and drastically shift device bandwidth.

The surface films are next patterned by reactive ion etching and wet etching as shown in Figure 2. Cr/Au metallization is sputtered on and patterned via liftoff to

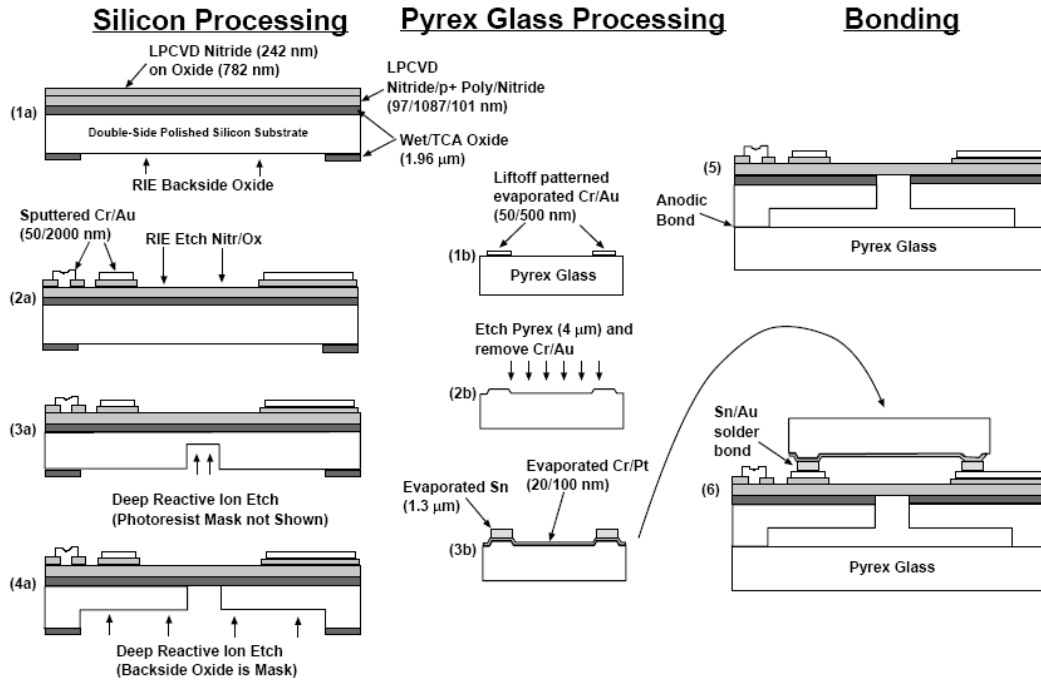


Figure 2: Diagram of the microfabrication process.

define the bond pads for the top glass die, the pads for connection to the package, and connections to the doped polysilicon layer. The wafers are then etched from the backside using deep reactive ion etching (DRIE). The first etch uses a photoresist mask and defines the membrane shapes, as shown in Figure 2 step 3a. A second DRIE etch is performed using the backside oxide as a hardmask, and stopping on the buried oxide etch stop. This etch defines the fluid chamber shape. The situation at this point is seen in Figure 2 step 4a. The buried oxide is then removed from the membrane regions in 1:1 HF, releasing the membranes.

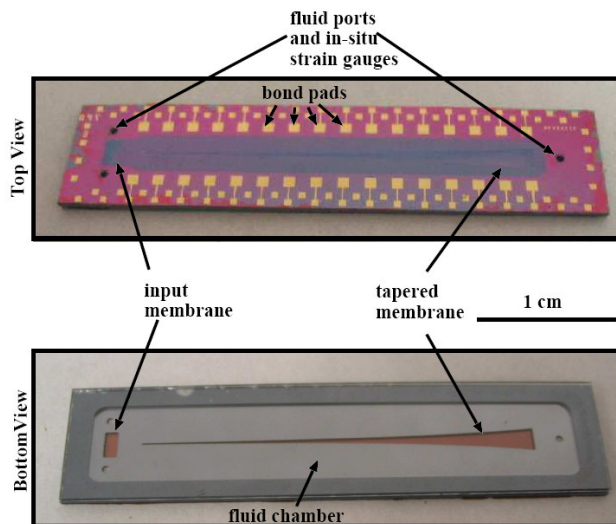


Figure 3: Photographs of the device after anodic bonding, but before bonding on the top electrode plate (that is, after step 5 in Figure 2).

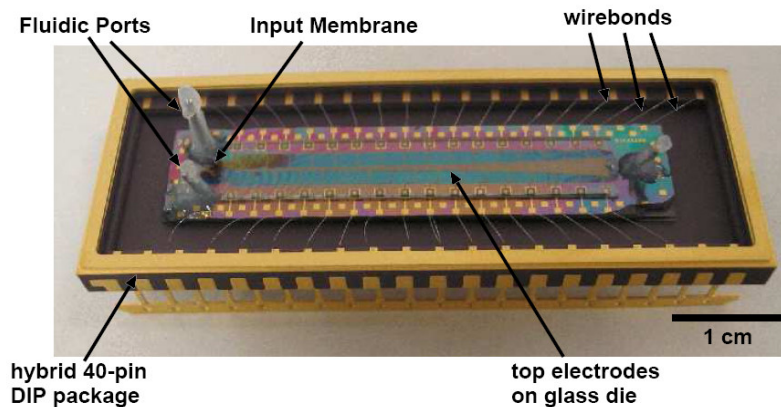


Figure 4: Photograph of the device with top glass plate bonded on, filled with fluid and sealed, and wirebonded into a DIP hybrid package.

In parallel with the silicon processing, a Pyrex glass wafer (Corning type 7740), is processed to produce the top electrodes for capacitive sensing. First, 4 μm high legs are etched into the glass using 3:1 HF and an evaporated Cr/Au mask. Cr/Pt electrodes and Sn bumps are then evaporated on and patterned using liftoff, as shown in Figure 2 step 3b.

Diced Pyrex glass pieces are anodically bonded onto the backside of the silicon at 330 $^{\circ}\text{C}$ and 700 V, sealing the fluid chambers. The Pyrex top pieces are bonded on using Sn-Au fluxless solder bonding at 350 $^{\circ}\text{C}$ with 15 MPa applied clamping force per unit area. The structure is now complete, and ready to be packaged. Needles are epoxied into the filling ports and silicone oil is injected using a microinjection jig. The needles are cut and sealed off with epoxy. The finished chip is then mounted into a hybrid 40-pin dual inline package (DIP) with epoxy and wirebonded to make electrical connection with Au wirebonds. Photographs of the finished device are shown in Figure 3 and Figure 4.

EXPERIMENTAL RESULTS

Measurement of the mechanical vibration of the tapered membrane structure in the μCAT is carried out using a laser Doppler velocimetry (LDV) system. The LDV system is composed of a Polytec OFV-301 sensor head, custom optics, and a computer controlled micropositioning stage. The experiments are carried out on a μCAT with no top plate and 10/50 nm of Cr/Au sputtered on to the entire top surface for reflectivity. The chip is mounted on the stage with rubberized clamps, and an acoustically baffled piezoelectric tweeter is placed over the front end of the chip, delivering approximately 100 dB SPL pure tone acoustic excitation in the 2 kHz-70 kHz band. A Larson-Davis 0.25" pressure microphone is used as a reference inside the baffle to measure the strength and phase of the excitation. The setup is diagrammed in Figure 5.

The centerline magnitude and phase of the membrane vibration are shown in Figure 6. In the 10-60 kHz band maximum membrane vibration is observed at a frequency dependent location. This frequency-position mapping is the primary cochlear-like phenomenon the system was designed to reproduce. The phase shows that traveling waves dominate, another cochlear-like feature.

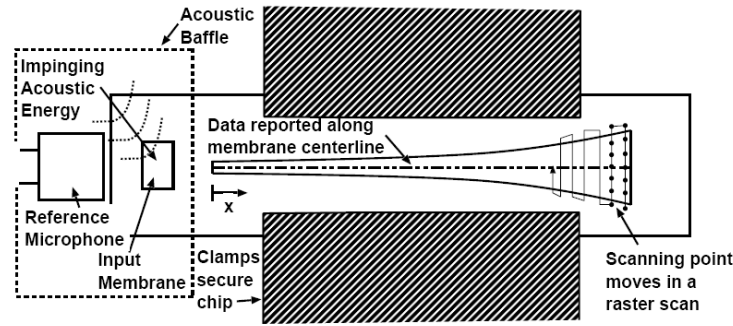


Figure 5: Diagram of mechanical measurement setup.

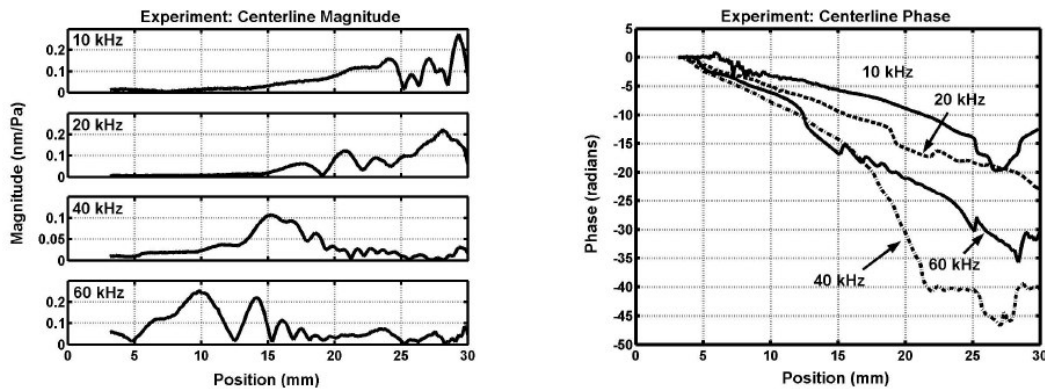


Figure 6: Experimental results along the membrane centerline. A frequency-position map and traveling wave are evident.

Commercial off-the-shelf components were used to construct the signal conditioning electronics for the μ CAT. The electronics are implemented on a custom PC board. There are three main functions for the electronics: (1) Generating a bias reference for the capacitive readout. (2) Multiplexing the 32 output channels to one of two preamplifiers. (3) Preamplifying the capacitive signal using a charge amp (at 100 mV/pC) and bandpass filter (with 40 dB of passband gain, 70 Hz-70 kHz bandwidth). Electrical sensitivity of the μ CAT was measured by driving a pure acoustic tone using the piezoelectric tweeter, and measuring the output from all 32 channels. The measurements were conducted for 9 V applied bias and for 0 V applied bias. With 0 V bias, any measured output should be electrical cross-talk from the speaker. Typical results are shown in Figure 7 for four driving frequencies. The measured sensitivities of the low frequency channels are 5-35 mV/Pa at the band pass filter output (0.05-0.35 mV/Pa at the preamp output). This is 100 times higher sensitivity than predicted by mathematical models of the system. Response is only seen from the channels at the wide end of the device. Very low sensitivity is seen for the narrow end channels, at all frequencies tested. (Tests were conducted from 2kHz-70kHz.) This also does not match model predictions, or expectations based on the frequency-position map observed in LDV experiments. The sensitivity reduces on all channels when the bias is set to zero, indicating that the measurements are recording true sensitivity to sound and not simply electrical cross-talk from the speaker drive.

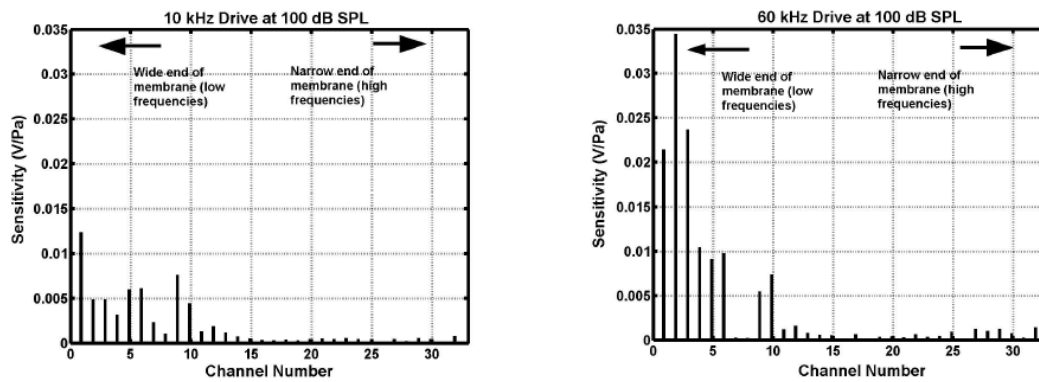


Figure 7: Electrical sensitivity of the 32 channels to two pure tone acoustic signals, at an applied bias level of 9V. Measurements are at the bandpass output.

It is not clear why the measured electrical sensitivity does not show the same shape as the mechanical motion measured by LDV. It is possible that only some of the Sn-Au bonds to the top electrodes are ohmic, causing only some of the channels to be connected. It is also possible that the acoustic baffling of the top Pyrex plate is insufficient, thus acoustic pressure is directly impinging on the tapered membrane.

CONCLUSIONS

The microscale cochlear analogue transducer (μ CAT) described here demonstrates the feasibility of a lifelike acoustic sensor which mimics the dynamics of the cochlea. This is an innovative approach to acoustic sensing, differing significantly from the traditional designs for hydrophones and microphones. Laser vibrometry measurements of the μ CAT dynamics demonstrated frequency-position mapping over the 10-60 kHz band with displacements on the order of 0.2 nm/Pa. Sensitivity measurements on the μ CAT indicate electrical sensitivity of the lower frequency channels (close to the wide end of the device) of 0.05-0.35 mV/Pa (at the preamp output).

At this point, no frequency-position mapping has been demonstrated in the electrical measurements. It is suspected that this is due to incomplete Sn-Au bonding of all channels, resulting in only some channels being connected. Another possibility is that the top Pyrex layer is not a sufficient acoustic baffle, so that incoming sound pressure is directly exciting motion of the tapered membrane, rather than mainly impinging on the device input.

The noise floor of the μ CAT is dominated by the preamp, mainly Johnson noise of the DC-stabilizing feedback resistor and the voltage noise of the operational amplifier. Improving the noise characteristics of the device would require improvements to this preamplifier stage. Additional improvements to sensitivity could be achieved by including a "middle ear" mechanical impedance matching network to improve coupling between the air and the trapped fluid.

The measured power consumption of the entire multichannel electronics is 326 mW, when operating off of +15 V and -15 V supplies. The preamplifiers and bandpass filters account for 92% of the power consumption of the device. Reduction in power could be achieved by operating at a lower voltage, perhaps

using a single 3.3 V or 5 V supply. This would result in a 10 dB reduction in sensitivity, but would be a worthwhile tradeoff for low power applications.

The major advantages of the μ CAT sensor system are its ability to perform mechanical signal analysis with low power requirements. Potential applications for the technology include unattended sensors in structural health monitoring, sensing for autonomous vehicles, and frontends for cochlear implants or hearing aids.

Additional work needs to be done on proving the sensor capabilities, particularly electrical sensing. Additional work on packaging is also needed. To achieve a truly cochlear-like filter, feedback mechanisms will need to be added to the system to mimic the operation of the Outer Hair Cell (OHC) mechanics. These mechanisms may also be used to impart orthotropic qualities to the structure and add damping, both of which can improve filter sharpness and peak sensitivity.

REFERENCES

1. Johnstone, B.M., *Genesis of the Cochlear Endolymphatic Potential*. Current Topics in Bioenergetics, 1967. **2**: p. 335-352.
2. Sarpeshkar, R., R.F. Lyon, and C. Mead, *A Low-Power Wide-Dynamic-Range Analog VLSI Cochlea*. Analog Integrated Circuits and Signal Processing, 1998. **16**(3): p. 245-274.
3. Dallos, P., A. Popper, and R. Fay, *The Cochlea*. Springer handbook of auditory research. Vol. 8. 1996: Springer, New York.
4. Chadwick, R.S., M.E. Fourney, and P. Neiswander, *Modes and waves in a cochlear model*. Hear. Res., 1980. **2**: p. 475-483.
5. Lechner, T.P., *A hydromechanical model of the cochlea with nonlinear feedback using PVF₂ bending transducers*. Hear. Res., 1993. **66**: p. 202-212.
6. Chen, F.Y., et al., *A hydromechanical biomimetic cochlea: Experiments and models*. Journal of the Acoustical Society of America, 2006. **119**(1): p. 394-405.
7. Hemmert, W., et al., eds. *A life-sized hydrodynamical, micromechanical inner ear*. Biophysics of the Cochlea: from Molecules to Models, ed. A.W. Gummer. 2002, World Scientific. 409-416.
8. Wittbrodt, M.J., C.R. Steele, and S. Puria, *Developing a Physical Model of the Cochlea Using Microfabrication Methods*. Audiology and Neuro-otology, 2006. **11**: p. 104-112.
9. Zhou, G., et al., *A life-sized physical model of the human cochlea with optical holographic readout*. J. Acoust. Soc. Am., 1993. **93**: p. 1516--1523.
10. White, R.D., *Biomimetic Trapped-fluid Microsystems for Acoustic Sensing*, in *Mechanical Engineering*. 2005, University of Michigan: Ann Arbor.
11. White, R.D. and K. Grosh, *Microengineered hydromechanical cochlear model*. Proceedings of the National Academy of Sciences, 2005. **102**: p. 1296-1301.
12. White, R.D. and K. Grosh. *Trapped-fluid traveling wave filters based on the mammalian cochlea*. in *Proceedings of microTAS 2005, the 9th International Conference on Miniaturized Systems for Chemistry and Life Science*. 2005.
13. White, R.D. and K. Grosh, *Fully micromachined lifeseize cochlear model*, in *Auditory Mechanisms: Processes and Models*, A.L. Nuttall, Editor. 2005: Portland, OR.
14. Finlayson, R.D., et al., *Health monitoring of aerospace structures with acoustic emission and acousto-ultrasonics*. Insight, 2001. **43**(3): p. 155-158.
15. Rizzo, P. and F.L. di Scalea, *Acoustic emission monitoring of carbon-fiber-reinforced-polymer bridge stay cables in large-scale testing*. Experimental Mechanics, 2001. **41**(3): p. 282-290.
16. Martin, W.N., et al., *An artificial neural receptor system for structural health monitoring*. Structural Health Monitoring-an International Journal, 2005. **4**(3): p. 229-245.
17. Kirikera, G.R., et al., *Damage localisation in composite and metallic structures using a structural neural system and simulated acoustic emissions*. Mechanical Systems and Signal Processing, 2007. **21**(1): p. 280-297.
18. Robles, L. and M.A. Ruggero, *Mechanics of the Mammalian Cochlea*. Physiol. Rev., 2001. **81**: p. 1305-1352.
19. Geisler, C.D., *From Sound to Synapse*. 1998: Oxford University Press.